ARL-RP-0527 ● AUG 2015

US Army Research Laboratory

Penetration Resistance of Armor Ceramics: Dimensional Analysis and Property Correlations

by JD Clayton

A reprint from the International Journal of Impact Engineering. 2015;85:124–131

NOTICES

Disclaimers

The findings in this report are not to be construed as an official Department of the Army position unless so designated by other authorized documents.

Citation of manufacturer's or trade names does not constitute an official endorsement or approval of the use thereof.

Destroy this report when it is no longer needed. Do not return it to the originator.

ARL-RP-0527 ● AUG 2015

US Army Research Laboratory

Penetration Resistance of Armor Ceramics: Dimensional Analysis and Property Correlations

by JD Clayton
Weapons and Materials Research Directorate, ARL

A reprint from the International Journal of Impact Engineering. 2015;85:124–131

REPORT DOCUMENTATION PAGE

Form Approved
OMB No. 0704-0188

1. REPORT DATE *(DD-MM-YYYY)*	2. REPORT TYPE	3. DATES COVERED (From - To)
August 2015	Reprint	January–July 2015

4. TITLE AND SUBTITLE
Penetration Resistance of Armor Ceramics: Dimensional Analysis and Property Correlations

5a. CONTRACT NUMBER

5b. GRANT NUMBER

5c. PROGRAM ELEMENT NUMBER

6. AUTHOR(S)
JD Clayton

5d. PROJECT NUMBER
AH80

5e. TASK NUMBER

5f. WORK UNIT NUMBER

7. PERFORMING ORGANIZATION NAME(S) AND ADDRESS(ES)
US Army Research Laboratory
ATTN: RDRL-WMP-C
Aberdeen Proving Ground, MD 21005-5069

8. PERFORMING ORGANIZATION REPORT NUMBER
ARL-RP-0527

9. SPONSORING/MONITORING AGENCY NAME(S) AND ADDRESS(ES)

10. SPONSOR/MONITOR'S ACRONYM(S)

11. SPONSOR/MONITOR'S REPORT NUMBER(S)

12. DISTRIBUTION/AVAILABILITY STATEMENT
Approved for public release; distribution is unlimited.

13. SUPPLEMENTARY NOTES
A reprint from the International Journal of Impact Engineering. 2015;85:124–131

14. ABSTRACT

A new dimensionless relationship for analysis of ballistic penetration data is derived and applied to polycrystalline ceramic materials. Targets consist of ceramic tiles backed by thick metallic plates within which residual penetration depths have been reported in experimental studies. Particular ceramics analyzed here are low- and high-purity alumina, aluminum nitride, boron carbide, silicon carbide, and titanium diboride. Data for penetration depth versus ceramic tile thickness tend to fall on lines of constant slope regardless of impact velocity, suggesting effects of penetrator velocity and tile thickness may be represented by a separable function of rank two for normalized depth of penetration. The particular relationship developed here contains two material parameters: a length scale and an energy per unit mass. Simultaneous consideration of results of the dimensional analysis and material properties suggest that the length scale, which is related to decreasing penetration depth with increasing tile thickness, correlates with the ratio of surface energy to elastic modulus. The energy per unit mass, which is linked to the relationship between penetration depth and penetrator velocity, correlates with dynamic shear strength of failed ceramic reported from plate impact experiments, divided by mass density. The dimensional analysis provides a structured framework under which future multiscale simulations and validation experiments can be organized and compared.

15. SUBJECT TERMS
ceramics, terminal ballistics, armor, dimensional analysis

16. SECURITY CLASSIFICATION OF:			17. LIMITATION OF ABSTRACT	18. NUMBER OF PAGES	19a. NAME OF RESPONSIBLE PERSON
a. REPORT	b. ABSTRACT	c. THIS PAGE			JD Clayton
Unclassified	Unclassified	Unclassified	UU	14	19b. TELEPHONE NUMBER (Include area code) 410-278-6146

International Journal of Impact Engineering 85 (2015) 124–131

Contents lists available at ScienceDirect

International Journal of Impact Engineering

journal homepage: www.elsevier.com/locate/ijimpeng

Penetration resistance of armor ceramics: Dimensional analysis and property correlations

J.D. Clayton [a, b, *]

[a] Impact Physics RDRL-WMP-C, US Army Research Laboratory, Aberdeen Proving Ground, MD 21005-5066, USA
[b] Adjunct Faculty, A. James Clark School of Engineering, University of Maryland, College Park, MD 20742, USA

ARTICLE INFO

Article history:
Received 20 February 2015
Received in revised form
18 June 2015
Accepted 20 June 2015
Available online 10 July 2015

Keywords:
Ceramics
Terminal ballistics
Armor
Dimensional analysis

ABSTRACT

A new dimensionless relationship for analysis of ballistic penetration data is derived and applied to polycrystalline ceramic materials. Targets consist of ceramic tiles backed by thick metallic plates within which residual penetration depths have been reported in experimental studies. Particular ceramics analyzed here are low- and high-purity alumina, aluminum nitride, boron carbide, silicon carbide, and titanium diboride. Data for penetration depth versus ceramic tile thickness tend to fall on lines of constant slope regardless of impact velocity, suggesting effects of penetrator velocity and tile thickness may be represented by a separable function of rank two for normalized depth of penetration. The particular relationship developed here contains two material parameters: a length scale and an energy per unit mass. Simultaneous consideration of results of the dimensional analysis and material properties suggest that the length scale, which is related to decreasing penetration depth with increasing tile thickness, correlates with the ratio of surface energy to elastic modulus. The energy per unit mass, which is linked to the relationship between penetration depth and penetrator velocity, correlates with dynamic shear strength of failed ceramic reported from plate impact experiments, divided by mass density. The dimensional analysis provides a structured framework under which future multiscale simulations and validation experiments can be organized and compared.

Published by Elsevier Ltd.

1. Introduction

Ceramic materials comprise important components of many modern protection systems for vehicles and personnel, i.e., vehicular armor and body armor. Experiments and numerical simulations of ballistic performance of armor ceramics have considered various projectile and target geometries, materials, and velocity regimes, as summarized in Ref. [1,2], for example. Popular experiments include those that measure limit velocities for complete perforation of monolithic or layered structures (i.e., V_{50}), those intended to monitor dwell in confined cylindrical targets, and those that measure penetration depth into a backing material, typically metallic, placed behind ceramic tile(s). Properties often deemed favorable include high hardness, high elastic stiffness, high strengths (static/dynamic compressive, shear, and bending), and low density relative to armor steels; drawbacks include brittleness and high cost. However, consensus regarding relative importance of ceramic material properties affecting results of experiments designed to inform protection applications remains elusive. Relationships among macroscopic properties and microstructure features are difficult to isolate and hence often unclear.

Efforts towards relating measurable properties to ballistic performance of brittle materials (e.g., ceramics and glass) have been undertaken since at least the 1960s. Comprehensive review articles on the subject in the context of armor ceramics include [1,3,4]; a few other notable works are mentioned here. In Ref. [5], correlation of performance with an average of the static and dynamic compressive strengths of the ceramic, normalized by mass density, was reported. In Ref. [6], it was suggested that ceramic hardness, fracture toughness (or surface energy), and penetration resistance may be related. In contrast, recent experiments [7] on various silicon carbides found depth of penetration to depend on hardness but not toughness. In Ref. [8], dynamic shear strength was inferred as an important property in ballistic penetration experiments; subsequent computational results [9] and data analysis [10] have further demonstrated important effects of friction and shear strength of the fractured or comminuted ceramic material when

* Impact Physics RDRL-WMP-C, US Army Research Laboratory, Aberdeen Proving Ground, MD 21005-5066, USA. Tel.: +1 410 278 6146; fax: +1 410 278 2460.
E-mail addresses: jdclayt1@umd.edu, john.d.clayton1.civ@mail.mil.

http://dx.doi.org/10.1016/j.ijimpeng.2015.06.025
0734-743X/Published by Elsevier Ltd.

impacted in the hypervelocity regime. In Ref. [11], flaw size, elasticity, plasticity, and fracture properties enter an analytical model for dwell based on a dimensionless ductility parameter [12]. Importance of both hardness and ductility (including inelastic deformation mediated by dislocations and/or micro-cracks) on transition velocities for dwell in confined thick ceramic targets was reported in Ref. [13].

Principles of dimensional analysis were formally established upon proof of Buckingham's pi theorem of the early 20th century [14]. Dimensional analysis enables a reduction in the number of independent variables that must be considered in a functional relationship among physical quantities observed in experiments. For example, if fundamental units of mass, length, and time are all involved independently, a reduction in the number of independent variables by three is possible. Detailed discussion and example applications in solid and fluid mechanics can be found in Refs. [15–17], with the latter [17] formalizing regimes in which self-similarity may describe a particular problem. Dimensional analysis may enable relating data collected from laboratory experiments conducted at one length/time scale to data collected from observations of physical phenomena at scales exceeding pragmatic reach of experimental facilities. It is noted, however, that the choice of dimensionless parameters is not unique, and physical insight is often obtained only from particular choices guided by logic and some additional knowledge, beyond the numerical data, of the problem under consideration.

The only previously published attempt incorporating formal dimensional analysis to relate ceramic material properties to ballistic performance in depth of penetration experiments known to the present author is reported in Ref. [18], wherein no strong correlations were discovered. However, this prior effort considered only a small scope of data available in years up to 1992 and focused primarily on static (but not dynamic) material properties. Perhaps further complicating (if not confusing) the analysis are simultaneous consideration of multiple performance metrics (e.g., penetration depth normalized in various ways) that lead to different rank orderings of material superiority for the same set of raw data. Complicating the general problem of analysis of ballistic penetration data on armor ceramics is the large number of factors [2,19–23] that may affect performance in addition to impact velocity, ceramic material, and total ceramic target thickness, including but not necessarily limited to the following: penetrator geometry, penetrator material, backing material, possible lateral confinement, possible face-plate or buffer, layers of thin versus thick tiles with possible binder material, lateral dimensions of tiles, and variability in ceramic material purity and initial defect content. Dimensional analysis has been applied towards penetration of mononlithic metallic targets by long rods with mixed success [2,24–26]. Recently, similitude analysis has been used to describe penetration of steel targets by tungsten alloy and hardened steel projectiles [27], including development of equations for predicting ballistic limit thickness and limit velocity, as well as residual projectile velocity and residual projectile length for overmatched targets.

The present paper offers the following new technical contributions. Recognizing that penetration depth versus ceramic target thickness data tend to fall on lines of constant slope regardless of impact velocity, an additively separable relationship for normalized depth of penetration is proposed. This relationship contains two material parameters: a length scale $\mathscr{L}$ and an energy per unit mass $\mathscr{E}$. The relationship is fit to penetration data from six experimental studies reported in the open literature [5,23,28–31] on six polycrystalline armor ceramics: low- and high-purity alumina (respectively labeled $Al_2O_3^-$ and $Al_2O_3^+$), aluminum nitride (AlN), boron carbide (B_4C), silicon carbide (SiC), and titanium diboride (TiB_2). In other words, parameters $\mathscr{L}$ and $\mathscr{E}$ are determined for each set of experimental data; different values are obtained among data sets because of different test geometries, backing materials, etc. These two parameters are correlated with ceramic material properties upon consideration of physics associated with each parameter via the way it enters the dimensionless equation. Results offer new insight into performance evaluation of armor ceramics in ballistic impact.

The main content of this paper is organized as follows. General concepts from dimensional analysis applicable to problems in penetration mechanics are considered in §2. Particular applications of these concepts towards ballistic penetration data on ceramics are addressed in §3. Relationships among parameters entering the dimensionless equation(s) and properties of ceramic materials are postulated in §4, with corresponding discussion. Conclusions follow in §5. Regarding notation, mathematical variables are written in italic or Greek font, with a definition of each variable given soon after it first appears in the text.

2. Dimensional analysis: general

In this paper, Buckingham's pi theorem is applied towards dimensional analysis of physical systems involving ballistic penetration. Firstly, Buckingham's pi theorem applied to any system can be stated as follows [14–16]. If an equation involving n variables is dimensionally homogeneous, it can be reduced to an equation among $n-k$ independent dimensionless products, with k being the number of independent reference dimensions needed to characterize all of the variables. In dimensional (rather than dimensionless) form, let

$$y = f(x_2, x_3, \ldots, x_n), \tag{2.1}$$

where y is the dependent variable and $x_2,\ldots, x_n$ are independent quantities, some of which may be independent variables and others constants in a given problem. Equation (2.1) can be transformed into dimensionless form as

$$\Pi_1 = \phi(\Pi_2, \Pi_3, \ldots, \Pi_{n-k}), \tag{2.2}$$

where Π_1 is the dimensionless version of y and function ϕ depends on $n - k - 1$ other dimensionless products (i.e., pi terms) constructed from the original set $\{y, x_2, x_3,\ldots, x_n\}$. Pragmatically, normalization of all variables entering ϕ should be performed using only the set $\{x_2, x_3,\ldots, x_n\}$ so that the independent variable y appears only once, on the left side of the equation.

The ballistic penetration problem to which Buckingham's theorem is applied herein is shown in Fig. 1(a). The experimental setup, as introduced for example in Ref. [5], consists of a projectile of initial length L_0 impacting a ceramic target of total thickness h at velocity V_0, with the ceramic target fronting a thick (effectively semi-infinite) metallic backing. The ceramic target may consist of one or more layered tiles. The present analysis is restricted to normal impact, i.e., effectively null obliquity. Performance of the ceramic is measured by residual penetration depth P, with penetration resistance decreasing with increasing P.

In dimensional form, penetration depth can be written as the following function of impact velocity, geometric variables $\{g\}$, and material property variables $\{m\}$, letting subscripts 0, T, B denote penetrator, ceramic tile, and backing metal:

$$P = P(V_0, \{g\}_0, \{m\}_0, \{g\}_T, \{m\}_T, \{g\}_B, \{m\}_B). \tag{2.3}$$

Possible lateral confinement is included in the sets of geometric variables for the tile and backing. In subsequent analysis, application/fitting of (2.3) is restricted to experimental data sets for which

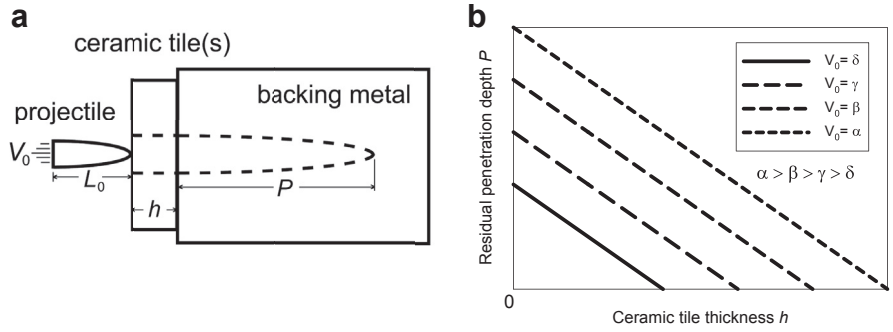

Fig. 1. Ballistic experiment (a) and typical fits to residual penetration data (b).

the backing and tile geometry remain fixed and the penetrator material remains fixed. Further letting $\{g\}_0 \to L_0$, $\{g\}_T \to h$, (2.3) reduces under these assumptions to

$$P = P(V_0, L_0, h, \{m\}_T, \{m\}_B). \tag{2.4}$$

A reduced form of (2.4) is needed in the context of dimensional analysis. This reduced equation should satisfy the following requirements: (i) it should be a dimensionless function of dimensionless quantities, (ii) it should yield the penetration depth into the bare backing material as $h \to 0$, and (iii) it should satisfy observed physics of the problem, notably a linearly decreasing penetration depth with increasing tile thickness, with the slope of P versus h constant among test data for different impact velocities with all other quantities (i.e., material properties and geometry) held fixed. The latter point is demonstrated visually in Fig. 1(b), and is characteristic of ceramic penetration data as noted in Ref. [2] and demonstrated later in results shown in §3. In order to satisfy these requirements with minimal complexity, three parameters are introduced: a reference velocity V_R that is used to normalize the impact velocity in the penetration depth relation for the bare backing material, a material length scale $\mathscr{L}$ that depends on the ceramic tile material, and an energy per unit mass $\mathscr{E}$ that also depends on the ceramic tile material. In other words, $\{m\}_T \to \{\mathscr{L},\mathscr{E}\}$ and $\{m\}_B \to V_R$. In dimensional form,

$$P = P(V_0, L_0, V_R, h, \mathscr{L}, \mathscr{E}). \tag{2.5}$$

Each application of (2.5) is further restricted to data sets for which the penetrator geometry is fixed, such that $L_0 =$ constant is used only to normalize P as is conventional in analysis of ballistic data [2,24,25], leading to the dimensionless form [requirement (i)]

$$P/L_0 = \phi\left(V_0/V_R, h/\mathscr{L}, \mathscr{E}\Big/V_R^2\right). \tag{2.6}$$

In the context of Buckingham's theorem, two independent dimensions (length and velocity) enter the variables considered in (2.5), so $k = 2$. Since L_0 is fixed and has units redundant with h, the total number of pi terms is $n = 6$, and the number of dependent dimensionless terms is thus $n - k - 1 = 3$, which is fully consistent with the number of dependent variables on the right side of dimensionless Equation (2.6). Requirement (ii) above implies

$$(P/L_0)_B = \phi(V_0/V_R, 0, 0) = \phi_B(V_0/V_R), \tag{2.7}$$

where ϕ_B is the dimensionless penetration depth into the pure backing metal. Requirement (iii) suggests a separable equation of the following form:

$$P/L_0 = \phi = \varphi(h/\mathscr{L}) + \psi\left(V_0/V_R, \mathscr{E}\Big/V_R^2\right), \tag{2.8}$$

where φ is linear in h, $\varphi(0) = 0$, and $\psi(V_0/V_R,0) = \phi_B$. Application of (2.8) to data in §3 demonstrate that a linear penetration depth versus impact velocity relation is sufficient to describe the bare backing metal over velocity regimes of interest, as will be shown explicitly later. The final form of (2.6) used herein thus becomes

$$\frac{P}{L_0} = -\frac{h}{\mathscr{L}} + c_0 + \frac{V_0}{V_R}\left(1 - \frac{\mathscr{E}}{V_R^2}\right). \tag{2.9}$$

Here, c_0 is a dimensionless constant entering the aforementioned linear fit to penetration data for the bare backing. Penetration depth decreases linearly with increasing tile thickness and increases with increasing $\mathscr{L}$. Increases in ceramic property $\mathscr{E}$ linearly reduce the velocity dependent component of residual penetration. Consider (2.8) and (2.9) applied to a data set for a fixed tile material, in which only V_0 and h vary among data points. The penetration depth equation is an example of a separable function of rank $p = 2$ of the general form [32]

$$\phi(h, V_0) = \sum_{i=1}^{p} \varphi_i(h)\psi_i(V_0), \tag{2.10}$$

where in particular here

$$\varphi_1 = \varphi = -h/\mathscr{L}, \quad \varphi_2 = 1; \quad \psi_1 = 1, \quad \psi_2 = \psi = c_0 + \frac{V_0}{V_R}\left(1 - \frac{\mathscr{E}}{V_R^2}\right). \tag{2.11}$$

The following properties then apply for partial derivatives of ϕ:

$$\frac{\partial\phi}{\partial h} = \sum_{i=1}^{p} \frac{\partial\varphi_i}{\partial h}\psi_i = \frac{\partial\varphi}{\partial h}; \quad \frac{\partial\phi}{\partial V_0} = \sum_{i=1}^{p} \frac{\partial\psi_i}{\partial V_0}\varphi_i = \frac{\partial\psi}{\partial V_0}. \tag{2.12}$$

For the linear functions $\varphi(h)$ and $\psi(V_0)$ in (2.11), Equation (2.12) can be solved for dimensional ceramic material parameters $\mathscr{L}$ and $\mathscr{E}$:

$$\mathscr{L} = -\frac{L_0}{\partial P/\partial h}; \quad \mathscr{E} = V_R^2\left(1 - \frac{V_R}{L_0}\frac{\partial P}{\partial V_0}\right). \tag{2.13}$$

Equations in (2.13) can be derived directly from (2.9) for the present case wherein $P = P(h,V_0)$ with other factors held constant. However, (2.10)–(2.12) imply how the approach could be extended to other more general kinds of separable functions. Note also that $\phi \neq \varphi$ in (2.12) unless $\psi = 0$.

3. Dimensional analysis: application to test data

For the backing metal alone (i.e., no tile), (2.9) reduces to

$$P/L_0 = c_0 + V_0/V_R. \tag{3.1}$$

A linear regression with fit quality denoted conventionally by R^2 is applied to determine intercept c_0 and reference velocity (inverse slope) V_R for each data set commensurate with experiments listed in Table 1. Resulting values are shown in Table 3. Sufficiency of the linear fits is demonstrated, for example, by representative results shown in Fig. 2. The quality of fits for which only two experimental data points are reported [28] is indeterminate.

Experimental configurations for which the final dimensionless form of residual penetration depth equation in (2.9) is applied are listed in Table 1. These consider various projectile types of lengths ranging from 12.7 to 72.5 mm and impact velocities ranging from 0.6 to 3.0 km/s. Backing metals consist of monolithic thick plates of various steels and aluminum alloys. Ceramic tiles include six different effectively isotropic polycrystalline materials: low purity alumina (e.g., AD-85), high purity alumina (e.g., AD-995), aluminum nitride, boron carbide, silicon carbide, and titanium diboride. Total tile thickness ranges from 1.3 to 100 mm. In some cases [28,30], experiments considered stacks of multiple thinner tiles of the same total thickness h as one or fewer thicker tiles; in such cases, the number of tiles did not appear to affect the ballistic penetration depth, in contrast to results reported in one different study [22].

Physical properties of interest are listed in Table 2 with supplementary references. Initial mass density ρ, elastic (Young's) modulus E, Poisson's ratio ν, fracture toughness K_C, compressive strength σ_C, bending strength σ_B, and Vicker's hardness H_V are examples of static material properties. The Hugoniot Elastic Limit (HEL) σ_H and dynamic shear strength τ of the shocked ceramic, the latter defined in Ref. [10] from the intersection of the elastic line with the failed strength curve of the shocked material, are examples of dynamic material properties. Lattice parameters are a and c. Although values of properties shown in Table 2 are deemed most physically representative of the ceramics tested experimentally, complete property sets require consideration of characterization data from multiple sources, and variations among properties for a given material are common as evidenced by ranges of static property values reported in Ref. [18], for example. All of these ceramics undergo fracture (transgranular and/or intergranular) when subjected to dynamic/shock loading of sufficient magnitude. Other known inelastic deformation mechanisms are listed for each material in the second column from the right. In particular, slip and twinning refer to dislocation glide and mechanical/deformation twinning [33], respectively. The phase change in AlN is a solid–solid transformation from hexagonal to cubic crystal structure that occurs at pressures around 20 GPa (more specifically, wurtzite to rocksalt [34]). Amorphization in B_4C is a stress-induced change from trigonal (i.e., rhombohedral) crystal structure to a non-crystalline solid phase (i.e., glass) thought to occur at ballistic impact stresses in excess of 23 GPa [35]. While fracture and other inelastic deformation mechanisms in Table 2 presumably affect dynamic properties (e.g., τ), reliable quantitative relationships between thresholds for microscopic mechanism activation and values of macroscopic properties remain elusive for most polycrystalline armor ceramics.

Equation (2.9) is applied separately to penetration data for each ceramic tile material considered in each experimental data set listed in Table 1. Specifically, material parameters $\mathscr{L}$ and $\mathscr{E}$ are fit for each such application as follows. A plot of P versus h provides an estimate of $\partial P/\partial h$, which is found to be fairly constant for each impact velocity V_0. A plot of P versus V_0 at fixed values of h gives an overall estimate of $\partial P/\partial V_0$, which is found to be fairly constant and not vary too strongly with thickness h. Then, Equations in (2.13) are used to determine an initial guess of each of $\mathscr{L}$ and $\mathscr{E}$. The two parameters $\mathscr{L}$and $\mathscr{E}$ are then adjusted manually, if needed, to provide a best fit to the normalized experimental penetration data. Results of the parameter fitting are listed in the rightmost two columns of Table 3; here $\mathscr{E}$ is multiplied by mass density to provide a result with the same dimensions as stress. Note that velocity dependent parameters are not available for the data provided in Ref. [5] because the penetration data for the bare metallic backing was not reported in that study.

Accuracy, or possible lack thereof, of the parameter fits is demonstrated by representative results in Fig. 3. Specifically shown in each part of Fig. 3 are a result for each of the six ceramic materials, encompassing data from all five references in Table 1 from which both $\mathscr{L}$ and $\mathscr{E}$ could be determined. Velocities V_0 are relatively constant for each distinct segmented curve shown in Fig. 3(a)–(d) wherein corresponding experiments V_0 was varied over a substantial range, allowing for multiple such curves. In Fig. 3(e) and (f), the range of impact velocities considered was too small to warrant construction of separate curves; instead, all data are shown along with linear fits that compare favorably despite substantial scatter among individual experimental data points. Agreement between model and experiment is considered close except for the case of titanium diboride in Fig. 3(d) wherein the model tends to overpredict penetration depth at the lowest impact velocity and underpredict depth at the highest velocity.

4. Material behavior

As a corollary to Buckingham's pi theorem, if a dimensional equation such as (2.1) relates a single independent and dependent variable ($n = 2$, $k = 1$), then both variables must have the same physical dimensions, and their dimensionless ratio must equal a constant, i.e.,

$$y = f(x_2) \Rightarrow \Pi_1 = y/x_2 = \text{constant}. \tag{4.1}$$

The present objective is exploration of physical meanings of parameters $\mathscr{L}$ and $\mathscr{E}$ introduced in §2 and fit to ballistic test data in §3. Specifically sought are correlations among these parameters (which vary among ceramic materials and experimental data sets) and measurable physical properties such as those listed in Table 2. Because $\mathscr{L}$ and $\mathscr{E}$ vary among experimental test configurations,

Table 1
Ballistic penetration experiments.

Experiment	Projectile	L_0 [mm]	V_0 [km/s]	Backing	h [mm]	Tile materials
Rosenberg & Yeshurun [5]	AP, steel core	12.7, 14.5	0.92–0.98	Al 2024-T351	6–10	$Al_2O_3^-$, $Al_2O_3^+$, B_4C, SiC, TiB_2
Hohler et al. [28]	Rod, sintered W	50, 72.5	1.2–3.0	HH steel	10–100	$Al_2O_3^+$
Senf et al. [29]	Ogive, W-C core	30	0.6–1.0	RHA steel	6.7–30	$Al_2O_3^-$, $Al_2O_3^+$
Reaugh et al. [30]	Cylinder, sintered W	25.4	1.35–2.65	4340 steel	6.2–60	$Al_2O_3^-$, $Al_2O_3^+$, AlN, B_4C, SiC, TiB_2
Moynihan et al. [31]	AP, steel core	35.3	0.82–0.86	Al 5083-H131	1.3–6.4	$Al_2O_3^+$, B_4C, SiC
Savio et al. [23]	AP, steel core	28.4	0.60–0.83	Al 7017	5.1–9.6	B_4C

Table 2
Representative ceramic material properties.

Material	Density ρ [g/cm^3]	Modulus E [GPa]	Poisson ratio ν	Tough K_C [MPa$\sqrt{\text{m}}$]	Compress σ_C [GPa]	Bend σ_B [GPa]	Hard H_V [GPa]	HEL σ_H [GPa]	Dyn. str. 2τ [GPa]	Structure c,a [nm]	Inelastic deformation	References
$Al_2O_3^-$	3.4	221	0.20	3.0	2.2	0.32	9.1	5.5	4.3	Trigonal 1.3, 0.5	Slip, twinning	[30,36,37]
$Al_2O_3^+$	3.8	373	0.23	4.5	2.6	0.38	14.1	7.6	5.3	(same)	(same)	[4,10,29]
AlN	3.2	315	0.24	2.7	2.1	0.35	11.5	9.4	6.0	Hexagonal 0.5, 0.3	Slip, phase change	[9,38,39]
B_4C	2.5	461	0.17	3.1	2.8	0.40	31.4	16.0	7.1	Trigonal 1.2, 0.6	Amorphization	[10,36,40]
SiC	3.2	453	0.16	5.1	3.4	0.40	27.4	15.7	11.4	Hexagonal 1.5, 0.3	Slip	[10,36,41]
TiB_2	4.5	521	0.10	5.5	3.0	0.38	25.0	15.0	13.0	Hexagonal 0.3, 0.3	Slip	[10,36,42]

Table 3
Parameter fits from dimensional analysis.

Experiment	c_0	V_R [km/s]	R^2	Ceramic	$\mathscr{L}$ [mm]	$\mathscr{E}\cdot\rho$ [GPa]
Hohler et al. [28] ($L_0 = 72.5$ mm) ($L_0 = 50.0$ mm)	−0.67	1.11	1 (two points)	$Al_2O_3^+$	120.8	0.38
	0.57	3.13	1 (two points)	$Al_2O_3^+$	62.5	2.32
Senf et al. [29]	−0.44	0.43	0.9983	$Al_2O_3^-$	50.0	0.019
				$Al_2O_3^+$	21.4	0.031
Reaugh et al. [30]	0.31	1.72	0.9637	$Al_2O_3^-$	36.3	−0.81
				$Al_2O_3^+$	31.8	−0.15
				AlN	23.1	−0.13
				B_4C	25.2	−0.10
				SiC	33.0	1.13
				TiB_2	25.4	0.72
Moynihan et al. [31]	−0.58	0.45	0.9882	$Al_2O_3^+$	3.78	−0.12
				B_4C	3.09	−0.09
				SiC	3.25	−0.06
Savio et al. [23]	−1.03	0.28	0.9997	B_4C	7.2	33.0
Rosenberg & Yeshurun [5]				$Al_2O_3^-$	9.3, 12.2	
(c_0, V_R, S: not available)				$Al_2O_3^+$	6.9, 8.1	
($\mathscr{L}$: 12.7 mm, 14.5 mm projectile)				B_4C	6.6, 7.0	
				SiC	6.0, 6.6	
				TiB_2	5.7, 6.3	

trends in their values among different materials can only be deduced by considering values for different materials for fixed experimental configurations, i.e., values fitted to data from different references cannot, in general, be quantitatively compared.

Let $\{\xi\}_T$ denote sets of physically measurable properties that are constant for a given ceramic tile material. Examples are listed in Table 2 with supplementary references, though such lists may be incomplete, i.e., other unlisted properties may also be important. For a fixed experimental configuration, sought are relations of the form

$$\mathscr{L} = \mathscr{L}(\{\xi\}_T); \quad \mathscr{E} = \mathscr{E}(\{\xi\}_T). \tag{4.2}$$

Without further assumptions, a dimensional analysis of (4.2) is fruitless. As the simplest possible attempt at further analysis, assume that each function depends most strongly on a single material property, to be determined. Then (4.1) yields

$$\mathscr{L}/\xi_1 = c_1; \quad \mathscr{E}/\xi_2 = c_2; \tag{4.3}$$

where ξ_i are ceramic properties and c_i are dimensionless constants, with $i = 1,2$.

First consider ξ_1, which must have dimensions of length. Noting that $\mathscr{L}$ enters only the velocity independent part of (2.9), a logical choice would be a ratio of static properties. The best correlation among possibilities that can be constructed from Table 2 is obtained from $\xi_1 = \Gamma/E$, where E is Young's elastic modulus and Γ is surface energy, related to fracture toughness K_C and Poisson's ratio ν via

$$\Gamma = K_C^2\left(1-\nu^2\right)\Big/(2E). \tag{4.4}$$

Other combinations with dimensions of length – e.g., Γ/H, K_C^2/E, K_C^2/σ_B, etc. – fail to yield trends or correlations with $\mathscr{L}$ as significant

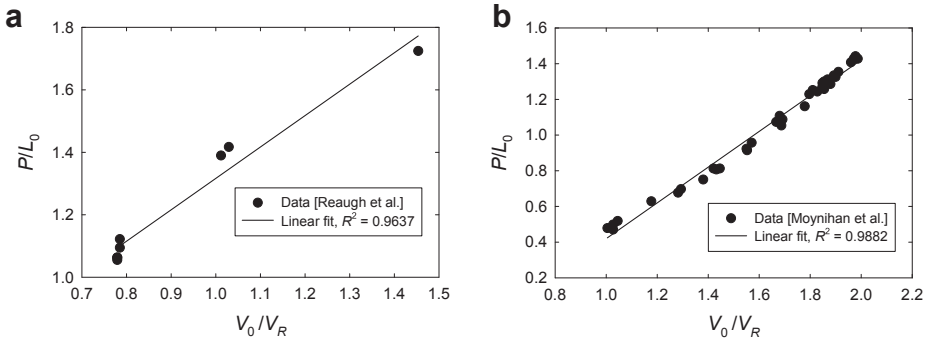

Fig. 2. Normalized residual penetration versus normalized penetrator velocity into bare backing metal with linear fits: (a) reference [30] (b) reference [31].

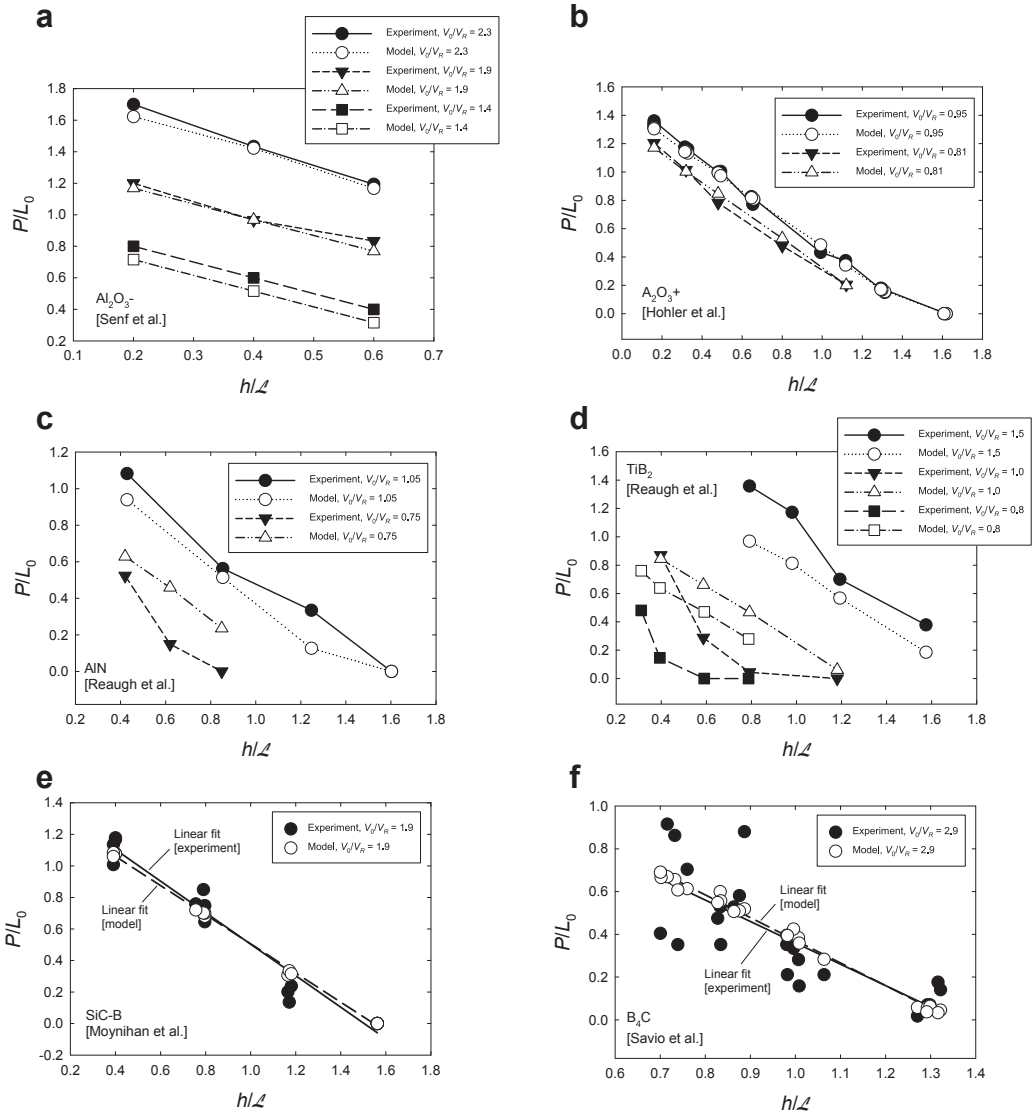

Fig. 3. Normalized residual penetration versus normalized total ceramic tile thickness, experimental data and model results: (a) $Al_2O_3^-$, data from Ref. [29] (b) $Al_2O_3^+$, data from Ref. [28] (c) AlN, data from Ref. [30] (d) TiB_2, data from Ref. [30] (e) SiC, data from Ref. [31] (f) B_4C, data from Ref. [23].

as those reported for Γ/E in what follows. A physical rationale for correlation between Γ/E and $\mathscr{L}$ is explained as follows. Recall from (2.9) and (2.13) that $\mathscr{L}$ scales the effect of tile thickness h on penetration depth. Ratio Γ/E can be interpreted as a measure of surface elastic energy to bulk elastic energy. As the ceramic target becomes thinner (smaller h), the importance of surface energy presumably becomes greater, as tensile fracture associated with bending becomes more likely [19,22]. Volumetric elastic energy becomes relatively more important for thicker targets, as the ratio of free surfaces to target volume decreases.

Now consider ξ_2, which must have dimensions of energy per unit mass or velocity squared. Noting that $\mathscr{E}$ only enters the velocity dependent part of (2.9), a logical choice would include dynamic material properties. The best correlation among possibilities that can be constructed from Table 2 is obtained from $\xi_2 = \tau/\rho$, where τ is dynamic shear strength as defined/reported in Ref. [10] for example, and ρ is mass density. The combination σ_H/ρ does not provide as satisfactory a correlation with $\mathscr{E}$, in agreement with the assessment of [10] that reported no correlation between the HEL of the ceramic tile and residual penetration depth. A physical rationale for correlation between τ/ρ and $\mathscr{E}$ is explained as follows. Recall from (2.9) and (2.13) that $\mathscr{E}$ scales the effect of penetrator velocity V_0 on penetration depth. Ratio τ/ρ can be interpreted as a measure of frictional sliding resistance or viscous stress supported by the failed or comminuted ceramic material [9,43,44]. Presuming that such resistance/stress depends on penetrator velocity would suggest correlation between dynamic shear strength and $\mathscr{E}$. Normalization by mass density is necessary to enable ξ_2 with the same dimensional units as $\mathscr{E}$.

Verification, or possible lack thereof, of the parameter–property correlations is considered in the context of Table 4, which only includes ballistic results in which multiple materials have been tested for the same experimental configuration. First consider $\mathscr{L}$: a smaller value of this parameter denotes stronger resistance to penetration as tile thickness h is increased. For each experimental data set, ceramics are listed from top to bottom in order of increasing $\mathscr{L}$. Values of Γ/E are listed side-by-side. Except for the three discrepancies marked in bold font, $\mathscr{L}$ and Γ/E increase in the same sequence. Low purity alumina always has a larger value of $\mathscr{L}$ than high purity alumina, and both aluminas tend to have larger

Table 4
Parameter-property correlations; discrepancies from general trends in bold font.

Experiment	Ceramic	$\mathscr{L}$ [mm]	$10^8\Gamma/E$ [mm]	Ceramic	$\mathscr{E}$ [J/g]	$10^{-3}\tau/\rho$ [J/g]
Senf et al. [29]	$Al_2O_3^+$	21.4	6.90	$Al_2O_3^+$	7.87	0.70
	$Al_2O_3^-$	50.0	8.85	$Al_2O_3^-$	5.25	0.63
Reaugh et al. [30]	AlN	23.1	3.47	SiC	358	1.78
	B_4C	25.2	**2.19**	TiB_2	160	1.44
	TiB_2	25.4	5.52	B_4C	−39	1.42
	$Al_2O_3^+$	31.8	6.90	AlN	−39	0.94
	SiC	33.0	**6.17**	$Al_2O_3^+$	−39	0.70
	Al_2O_3-	36.3	8.85	$Al_2O_3^-$	−238	0.63
Moynihan et al. [31]	B_4C	3.09	2.19	SiC	−20	1.78
	SiC	3.25	6.17	$Al_2O_3^+$	−33	0.70
	$Al_2O_3^+$	3.78	6.90	B_4C	−35	**1.42**
Rosenberg & Yeshurun [5]	TiB_2	6.0	5.52			
($\mathscr{L}$: average for two penetrator types)	SiC	6.3	6.17			
($\mathscr{E}$: not available from test data)	B_4C	6.8	**2.19**			
	$Al_2O_3^+$	7.5	6.90			
	$Al_2O_3^-$	10.8	8.85			

values than the other ceramics. Aluminum nitride data is available from only one data set [30] but corresponds to the lowest value of $\mathscr{L}$ for that set. Titanium diboride always has a larger value than silicon carbide. Data for boron carbide are inconsistent and represent two of the three anomalies from the proposed correlation.

Now consider $\mathscr{E}$, where larger values denote improved penetration resistance (decreasing P/L_0) with increasing velocity V_0 in (2.9). In the rightmost three columns of Table 4, ceramics are organized within each data set from top to bottom in concert with decreasing $\mathscr{E}$. Corresponding values of τ/ρ are given as well, demonstrating increasing (or at least stationary values of) $\mathscr{E}$ with increasing τ/ρ except for the lone data point in bold. In two of three data sets, alumina has the lowest value (i.e., worst performance), and low purity alumina always has a lower value than high purity alumina. Silicon carbide demonstrates superior performance to the other ceramics in both data sets in which it appears. The lone anomaly from the correlation again pertains to boron carbide, which has a lower value of $\mathscr{E}$ but higher value of τ/ρ than alumina considered in Ref. [31].

Perhaps unsurprisingly, three of four deviations from proposed correlations arise for boron carbide, whose dynamic behavior is notably difficult to characterize [45,46]. Some experimental configurations may lead to stress-induced amorphization in the tile while others may not; [5,30,31] do not provide microstructural characterization of the perforated tiles sufficient to support or reject this conjecture.

Experimental data exist for depth of penetration versus time for confined semi-infinite ceramic targets impacted by high velocity tungsten long rods, specifically confined targets of alumina [47], aluminum nitride [48], boron carbide [49], and silicon carbide [50]. Impact velocities were systematically varied from approximately 1.5 to 5.0 km/s in these experiments, with all other factors apart from the ceramic material essentially held fixed. Though particular Equations (2.3)–(2.13) would not apply towards this data (since there is no backing metal), a dimensional analysis similar to that invoked in the present paper could be applied to analyze such data, perhaps also incorporating parameters similar to $\mathscr{L}$ and $\mathscr{E}$. Such an exercise might give further insight into validity of the parameter property correlations proposed here in §4 of the present paper.

The dimensional analysis and resulting dimensionless equations for penetration depth developed in this paper provide a framework for systematic future research. A suite of additional ballistic experiments is recommended that would supplement those considered already, consisting of the same penetrator and backing material in each experiment, and varying the ceramic material, ceramic tile thickness, and penetrator velocity. Material properties should be measured as necessary such that uncertainties in these properties are eliminated, and then property–performance correlations posited originally in this work can be more strongly validated, or possibly refined/adjusted or refuted. Numerical simulations as in Refs. [2,9,30] are suggested as a means to provide further insight into possible correlations since physical properties can be varied independently, and at low cost, among simulations on (hypothetical) ceramic materials that may not be readily available for ballistic testing. Mesoscale (i.e., microstructure resolution) simulations relating structure and properties or property ratios, for example as described in Refs. [51–60], can then be used to suggest links between material property ratios entering the dimensional analysis and features of microstructure such as grain size, grain boundary strength, crystallographic texture, etc. For example, of particular relevance to dimensional parameter $\mathscr{E}$ is previous work in which mesoscale simulations of polycrystals were used to compute dynamic shear strength (e.g., τ) [55,58]. An overall strategy can be written as

$$\begin{array}{ccccccc} \text{ballistic} & & \text{dimensional} & & \text{material} & & \text{microstructure} \\ \text{performance} & \overset{1}{\leftrightarrow} & \text{parameters} & \overset{2}{\leftrightarrow} & \text{properties} & \overset{3}{\leftrightarrow} & (\text{grain size}, \\ (P/L_0) & & (\mathscr{L}, \mathscr{E}) & & (\Gamma/E, \tau/\rho) & & \text{orientation}\ldots) \end{array}$$

where arrows ↔denote links or correlations. Links labeled 1 and 2 have been formulated in the present paper; link 3, requiring consideration of microstructure characterization data (experimental and/or results from aforementioned multiscale simulations) remains to be addressed in more detail in future work.

5. Conclusions

Principles of dimensional analysis have been applied towards a study of ballistic penetration resistance of ceramic materials. In particular, data of study involve residual penetration depths into thick metallic backing plates fronted by ceramic tiles of alumina (low and high purity), aluminum nitride, boron carbide, silicon carbide, or titanium diboride. Data sets from six independent experimental investigations reported in the literature have been analyzed.

Application of Buckingham's pi theorem along with several physical assumptions has led to a dimensionless penetration depth relation depending on penetrator velocity, ceramic target thickness, and two material parameters unique to the ceramic material when other aspects of the test configuration (e.g., penetrator geometry and backing material) are held fixed in an experimental series. These parameters are a material length scale, which is related to the

thickness dependence of penetration resistance of the tiles, and an energy per unit mass, related to the velocity dependence of penetration resistance. Values of the two parameters have been determined via fitting the dimensionless relation to data sets for the six materials from the experimental investigations. Comparison of trends in values among different materials in a given investigation with trends in conventionally measured ceramic material properties has suggested correlation between the length scale and surface (fracture) energy divided by elastic modulus and correlation between the energy per unit mass and dynamic shear strength divided by initial mass density. Suggestions for future investigations involving numerical simulations at multiple length scales have been outlined that would provide further insight and more definitive relationships among structure, properties, and performance in the context of the dimensionless framework.

References

[1] Walley SM. Historical review of high strain rate and shock properties of ceramics. Adv Appl Ceram 2010;109:446–66.
[2] Rosenberg Z, Dekel E. Terminal ballistics. Berlin: Springer; 2012.
[3] Kaufmann C, Cronin D, Worswick M, Pageau G, Beth A. Influence of material properties on the ballistic performance of ceramics for personal body armour. Shock Vib 2003;10:51–8.
[4] Karandikar PG, Evans G, Wong S, Aghajanian MK. A review of ceramics for armor applications. Ceram Eng Sci Proc 2009;29:163–75.
[5] Rosenberg Z, Yeshurun Y. The relation between ballistic efficiency and compressive strength of ceramic tiles. Int J Impact Eng 1988;7:357–62.
[6] Sternberg J. Material properties determining the resistance of ceramics to high velocity penetration. J Appl Phys 1989;65:3417–24.
[7] Flinders M, Ray D, Anderson A, Cutler RA. High-toughness silicon carbide as armor. J Amer Ceram Soc 2005;88:2217–26.
[8] Rosenberg Z, Bless SJ, Brar NS. On the influence of the loss of shear strength on the ballistic performance of brittle solids. Int J Impact Eng 1990;9:45–9.
[9] Curran DR, Seaman L, Cooper T, Shockey DA. Micromechanical model for comminution and granular flow of brittle material under high strain rate application to penetration of ceramic targets. Int J Impact Eng 1993;13:53–83.
[10] Bourne NK. The relation of failure under 1D shock to the ballistic performance of brittle materials. Int J Impact Eng 2008;35:674–83.
[11] LaSalvia JC. Recent progress on the influence of microstructure and mechanical properties on ballistic performance. Ceram Trans 2002;134:557–70.
[12] Horii H, Nemat-Nasser S. Brittle failure in compression: splitting, faulting, and ductile-brittle transition. Phil Trans R Soc Lond A 1986;319:337–74.
[13] McCauley JW, Swab JJ, Hilton CD, Shanholtz ER, Portune AR. Quantifying bulk plasticity and predicting transition velocities for armor ceramics using hardness indentation tests. MD: US Army Research Laboratory, Aberdeen Proving Ground; 2012. Technical Report ARL-TR-6050.
[14] Buckingham E. On physically similar systems: illustrations of the use of dimensional equations. Phys Rev 1914;4:345–76.
[15] Bridgman PW. Dimensional analysis. New Haven: Yale University Press; 1931.
[16] Sedov LI. Similarity and dimensional methods in mechanics. London: Academic Press; 1959.
[17] Barenblatt GI. Similarity, self-similarity, and intermediate asymptotics. New York: Consultants Bureau, Plenum; 1979.
[18] Ernst H-J, Hoog K. Protective power of several ceramics correlated to some static material parameters. In: Proceedings 13th international symposium on ballistics, vol. 3; 1992. p. 119–26. Stockholm, Sweden.
[19] Woodward RL. A simple one-dimensional approach to modelling ceramic composite armour defeat. Int J Impact Eng 1990;9:455–74.
[20] Woodward RL, Baxter BJ. Ballistic evaluation of ceramics: influence of test conditions. Int J Impact Eng 1994;15:119–24.
[21] Rosenberg Z, Dekel E, Hohler V, Stilp AJ, Weber K. Penetration of tungsten-alloy rods into composite ceramic targets: experiments and 2-D simulations. In: Schmidt S, Dandekar D, Forbes J, editors. AIP conference proceedings, vol. 429. New York: AIP Press; 1998. p. 917–20.
[22] Yadav S, Ravichandran G. Penetration resistance of laminated ceramic/polymer structures. Int J Impact Eng 2003;28:557–74.
[23] Savio SG, Ramanjaneyulu K, Madhu V, Bhat TB. An experimental study on ballistic performance of boron carbide tiles. Int J Impact Eng 2011;38:535–41.
[24] Wright TW. A survey of penetration mechanics of long rods. In: Brebbia CA, Orszag SA, editors. Lecture notes in engineering: computational aspects of penetration, vol. 3. Berlin: Springer-Verlag; 1983.
[25] Anderson CE, Walker JD. An analytic expression for P/Lfor WA long rods into armor steel. In: Schmidt SC, Tao WC, editors. AIP conference proceedings, vol. 370. New York: AIP Press; 1996. p. 1135–8.
[26] Rosenberg Z, Dekel E. Material similarities in long-rod penetration mechanics. Int J Impact Eng 2001;25:361–72.
[27] Anderson CE, Riegel JP. A penetration model for metallic targets based on experimental data. Int J Impact Eng 2015;80:24–35.
[28] Hohler V, Stilp AJ, Weber K. Hypervelocity penetration of tungsten sinter-alloy rods into aluminum. Int J Impact Eng 1995;17:409–18.
[29] Senf H, Strassburger E, Rothenhausler H, Lexow B. The dependency of ballistic mass efficiency of light armor on striking velocity of small caliber projectiles. In: Proceedings 17th international symposium on ballistics, vol. 3; 1998. p. 199–206. Midrand, South Africa.
[30] Reaugh JE, Holt AC, Wilkins ML, Cunningham BJ, Hord BL, Kusubov AS. Impact studies of five ceramic materials and pyrex. Int J Impact Eng 1999;23:771–82.
[31] Moynihan TJ, Chou S-C, Mihalcin AL. Application of the depth-of-penetration test methodology to characterize ceramics for personnel protection. MD: US Army Research Laboratory, Aberdeen Proving Ground; 2000. Technical Report ARL-TR-2219.
[32] Rosenberg M. Separable functions and the generalization of matricial structure. Math Mag 1969;42:175–86.
[33] Clayton JD. Nonlinear mechanics of crystals. Dordrecht: Springer; 2011.
[34] Kato R, Hama J. First-principles calculation of the elastic stiffness tensor of aluminum nitride under high pressure. J Phys Condens Matter 1994;6:7617–32.
[35] Chen M, McCauley JW, Hemker KJ. Shock-induced localized amorphization in boron carbide. Science 2003;299:1563–6.
[36] Holmquist TJ, Rajendran AM, Templeton DW, Bishnoi KD. A ceramic armor material database. Warren, MI: US Army TARDEC; 1999. Technical Report 13754.
[37] Clayton JD. A continuum description of nonlinear elasticity, slip and twinning, with application to sapphire. Proc R Soc Lond A 2009;465:307–34.
[38] Hu G, Chen CQ, Ramesh KT, McCauley JW. Mechanisms of dynamic deformation and dynamic failure in aluminum nitride. Acta Mater 2012;60:3480–90.
[39] Anton RJ, Subhash G. Dynamic Vickers indentation of brittle materials. Wear 2000;239:27–35.
[40] Clayton JD. Towards a nonlinear elastic representation of finite compression and instability of boron carbide ceramic. Philos Mag 2012;92:2860–93.
[41] Clayton JD. Modeling nonlinear electromechanical behavior of shocked silicon carbide. J Appl Phys 2010;107(013520).
[42] Clayton JD. Finite strain analysis of shock compression of brittle solids applied to titanium diboride. Int J Impact Eng 2014;73:56–65.
[43] Grady DE. Shock-wave compression of brittle solids. Mech Mater 1998;29:181–203.
[44] Clayton JD. Deformation, fracture, and fragmentation in brittle geologic solids. Int J Fract 2010;163:151–72.
[45] Grady DE. Adiabatic shear failure in brittle solids. Int J Impact Eng 2011;38:661–7.
[46] Clayton JD, Tonge AL. A nonlinear anisotropic elastic–inelastic constitutive model for polycrystalline ceramics and minerals with application to boron carbide. Int J Solids Struct 2015;64–65:191–207.
[47] Subramanian R, Bless SJ. Penetration of semi-infinite AD995 alumina targets by tungsten long rod penetrators from 1.5 to 3.5 km/s. Int J Impact Eng 1995;17:807–16.
[48] Orphal DL, Franzen RR, Piekutowski AJ, Forrestal MJ. Penetration of confined aluminum nitride targets by tungsten long rods at 1.5–4.5 km/s. Int J Impact Eng 1996;18:355–68.
[49] Orphal DL, Franzen RR, Charters AC, Menna TL, Piekutowski AJ. Penetration of confined boron carbide targets by tungsten long rods at impact velocities from 1.5 to 5.0 km/s. Int J Impact Eng 1997;19:15–29.
[50] Orphal DL, Franzen RR. Penetration of confined silicon carbide targets by tungsten long rods at impact velocities from 1.5 to 4.6 km/s. Int J Impact Eng 1997;19:1–13.
[51] Bourne NK. Impact on alumina. I. Response at the mesoscale. Proc R Soc Lond A 2006;462:3061–80.
[52] Bourne NK. Impact on alumina. II. Linking the mesoscale to the continuum. Proc R Soc Lond A 2006;462:3213–31.
[53] Clayton JD, McDowell DL. A multiscale multiplicative decomposition for elastoplasticity of polycrystals. Int J Plast 2003;19:1401–44.
[54] Clayton JD. Dynamic plasticity and fracture in high density polycrystals: constitutive modeling and numerical simulation. J Mech Phys Solids 2005;53:261–301.
[55] Clayton JD, Kraft RH, Leavy RB. Mesoscale modeling of nonlinear elasticity and fracture in ceramic polycrystals under dynamic shear and compression. Int J Solids Struct 2012;49:2686–702.
[56] Clayton JD. Mesoscale modeling of dynamic compression of boron carbide polycrystals. Mech Res Comm 2013;49:57–64.
[57] Foulk JW, Vogler TJ. A grain-scale study of spall in brittle materials. Int J Fract 2010;163:225–42.
[58] Leavy RB, Clayton JD, Strack OE, Brannon RM, Strassburger E. Edge on impact simulations and experiments. In: Procedia engineeringvol. 58. Elsevier; 2013. p. 445–52.
[59] Kraft RH, Molinari JF. A statistical investigation of the effects of grain boundary properties on transgranular fracture. Acta Mater 2008;56:4739–49.
[60] Kraft RH, Molinari JF, Ramesh KT, Warner DH. Computational micromechanics of dynamic compressive loading of a brittle polycrystalline material using a distribution of grain boundary properties. J Mech Phys Solids 2008;56:2618–41.

1 (PDF) DEFENSE TECHNICAL INFORMATION CTR DTIC OCA

2 (PDF) DIRECTOR US ARMY RESEARCH LAB RDRL CIO LL IMAL HRA MAIL & RECORDS MGMT

1 (PDF) GOVT PRINTG OFC A MALHOTRA

46 (PDF) DIR USARL
RDRL CIH C
J KNAP
L MUNDAY
X WANG
RDRL WM
B FORCH
S KARNA
J MCCAULEY
RDRL WML B
I BATYREV
B RICE
D TAYLOR
N WEINGARTEN
RDRL WML H
B AYDELOTTE
D MALLICK
C MEYER
B SCHUSTER
RDRL WMM
J BEATTY
RDRL WMM B
G GAZONAS
D HOPKINS
B LOVE
B POWERS
C RANDOW
T SANO
R WILDMAN
RDRL WMM E
J LASALVIA
J SWAB
RDRL WMM F
M TSCHOPP
RDRL WMM G
J ANDZELM
RDRL WMP
S SCHOENFELD
RDRL WMP B
C HOPPEL
S SATAPATHY
M SCHEIDLER
A SOKOLOW
T WEERISOORIYA
RDRL WMP C
R BECKER
S BILYK
T BJERKE
D CASEM
J CLAYTON
D DANDEKAR
M FERMEN-COKER
M GREENFIELD
R LEAVY
J LLOYD
S SEGLETES
A TONGE
C WILLIAMS
RDRL WMP D
R DONEY

INTENTIONALLY LEFT BLANK.